공학석사 학위논문

Capacity fading mechanism of thick electrode in Lithium-ion rechargeable batteries

리튬이온 이차전지에서 후막 전극의
수명 열화 현상에 대한 연구

2019년 7월

서울대학교 대학원
재료공학부
박 지 원

Capacity fading mechanism of thick electrode in Lithium-ion rechargeable batteries

리튬이온 이차전지에서 후막 전극의
수명 열화 현상에 대한 연구

지도 교수 강 기 석

이 논문을 공학석사 학위논문으로 제출함

2019년 7월

서울대학교 대학원

재료공학부

박 지 원

박 지 원의 석사 학위논문을 인준함

2019년 07월

위 원 장 박 병 우 (인)

부위원장 강 기 석 (인)

위 원 김 미 영 (인)

Abstract

Capacity fading mechanism of thick electrode in Lithium-ion rechargeable batteries

Ji-won Park
Department of Material Science and Engineering
College of Engineering
The Graduate School
Seoul National University

In order to achieve the higher energy density batteries, increasing loading level of cathode material is considered as a promising method in the practical point of view. However, when the loading level of cathode material increases, capacity retention of the electrode significantly deteriorates. In this study, two different loading levels of cathode material (20 mg cm^{-2} and 28 mg cm^{-2} of $LiNi_{0.6}Co_{0.2}Mn_{0.2}O_2$, NCM622) are prepared as models for the study and I found that the state of charge inhomogeneity of 28 mg cm^{-2} loading level electrode is much severer

than that of 20 mg cm^{-2}. Furthermore, I found that of NCM622 near separator side actively oxidize/reduces, while the particles being near the current collector remains almost inert in 28 mg cm^{-2} electrode. Such discrepancy between separator and current collector side in 28 mg cm^{-2} electrode can be explained by sluggish ion transport in thick electrode after cycling. In case of charging, Li-ion is difficult to be extracted from the active material near the current collector side due to elongated Li-ion pathway in 28 mg cm^{-2} electrode. In case of discharging, Li-ion from electrolyte cannot reach to active material near the current collector side. Therefore, the active materials near the separator side participates the reaction more vigorously than current collector side ones, leading to the severe capacity fading of thick electrode due to its current hot spot. Here, I studied the relationships with the state of charge inhomogeneity and capacity fading of thick $LiNi_{0.6}Co_{0.2}Mn_{0.2}O_2$ electrode.

Keywords: Li-ion rechargeable batteries; layered oxide; thick electrode; state of charge inhomogeneity; capacity fading

Student Number: 2017-29935

Contents

List of Figures

Figure 8. Ex-situ XRD patterns every 25 cycles. The patterns of separator and current collector side were overlaid. (a) After charged, N20. (b) After charged, H28. (c) After discharged, N20. (d) After discharged, H28. There were no Al peaks on the patterns of the separator sides, while they were clearly observed on the patterns of the separator side

Figure 9. The calculated Li quantities from lattice parameter by full pattern matching method every 25 cycles. (a) N20. (b) H28.

Figure 10. SEM images of secondary active particles after 100 cycles. (a) N20, separator side. (b) N20, current collector side. (c) H28, separator side. (d) H28, current collector side.

Figure 11. The amount of electrolyte by-products measured by XPS after 100 cycles. (a) N20, separator side. (b) N20, current collector side. (c) H28, separator side. (d) H28, current collector side.

Figure 12. Impedance measurements every 20 cycles by EIS for (a) N20 (b) H28.

Figure 13. Cyclability test with different current density.

Figure 14. Cyclability test with different charge/discharge protocols. The upper part is for constant-current and constant-voltage mode (CCCV). The lower part is for constant-current mode (CC).

Figure 15. Suggested the capacity fading mechanism of thick electrode.

Chapter 1. Introduction

1.1 Motivation and outline

Nowadays, the human being is facing a variety of environmental problems, such as global warming and accelerated depletion of fossil fuels. The alternative solution to these problems is to replace the energy source from the fossil fuels into sustainable energy resources in various industries such as automobile and housing industry. Accordingly, the electric vehicles (EVs) is considered as a future oriented-technology to reduce the total use of fossil fuels of transportation. However, the current EVs has not fully met the demand of total driving mileages compared to the internal combustion engine based vehicles, because the practical energy density of Li-ion batteries, which is utilized in state-of-the-art EVs, is still far away from the long-distance drive requirements[1,2]. Thus, the new strategies on increasing total specific/volumetric energy density of Li-ion battery are intensively suggested for commercializing EVs, and it could be classified into the two major streams as following; (i) investigation on new electrode materials intrinsically possessing the high energy density[3-6] and (ii) improvement in the active material packing to increase the actual energy density of batteries[4-11]. Former has been demonstrated in various chemistries with Li-ions, such as Li-O_2 and Li-S. However, those systems have faced challenging to commercialize such as severe serious voltage hysteresis between charge/discharge, poor cyclability, and dissolution of active material and shuttling

effect[3-5]. In latter case, some trials have also been carried out. The previous studies reported that thick electrodes could practically provide higher energy density but exhibit poor power capability and significant capacity fading. The previous researchers, however, lack clear understanding behind the compromised electrochemical performance[10-16]. For example, K. Kitada *et al.* showed state of charge (SOC) inhomogeneity of active material in thick electrode only in first cycle[15]. In addition, indirect method for characterizing SOC inhomogeneity of active materials such as X-ray Diffraction (XRD)[15], or mathematical modeling are conducted to address the poor electrochemical performance[13].

In this study, SOC inhomogeneity is directly observed by Laser Induced Breakdown Spectroscopy (LIBS) and the SOC inhomogeneity is measured throughout the cycle life of thick electrode. Severe structural destruction of thick electrode in separator side is detected through SEM after 100 cycles. Moreover, byproducts from electrolyte is observed through XPS analysis. The structural destruction and byproducts from electrolyte significantly increased impedance in thick electrode and are confirmed through EIS analysis. These investigations are expected to play a key role in improving electrochemical performance of thick electrodes and contribute to developing high energy density battery.

Chapter 2. Experimental section

2.1 Electrode preparation and electrochemical analysis

NCM622 powder (provided by industrial partner), denka carbon black, and polyvinylidene fluoride (PVDF) were mixed in a weight ratio of 97:1.5:1.5 and added to *N*-methyl-2-pyrrolidone (NMP, anhydrous, 99.5%, Aldrich) for the electrode preparation. After this mixture was homogenized into a slurry, it was coated onto aluminum foil using the doctor-blade, dried 20 minutes in a 120 ℃ convection oven, and pressed by a roll-pressing machine. Coin-type half cells (CR2032, Wellcos) were assembled using the composite electrode as cathode, a lithium metal as an anode, glass fiber filter (GF/F) separator, and 1M $LiPF_6$ in ethylene carbonate/dimethyl carbonate (EC/DMC, 1:1 v/v, PanaX Etec) as the electrolyte. Galvanostatic measurements of the charge/discharge of the Li/NCM622 half-cells were conducted within the voltage range between 2.8 and 4.3 V with two different types of modes. First is constant-current mode (CC) whose current density is 150 mA g^{-1} (~1 C). Second is constant-current and constant-voltage mode (CCCV) whose current density is 150 mA g^{-1} and keeps the constant voltage at 2.8 and 4.3 V until the absolute current density becomes 3 mA g^{-1} (~0.02 C). Those electrochemical tests were conducted at 25 ℃ using a multichannel potentio-galvanostat (WBCS-3000, Wonatech, Korea).

2.2 Laser induced breakdown spectroscopy

State of Charge (SOC) inhomogeneity was observed by Laser Induced Breakdown Spectroscopy (LIBS, J200, Applied Spectra). LIBS is a quantitative elemental analysis that high power laser is induced on a sample and make the sample into plasma state. The plasma state materials return to ground state, emitting characteristic wavelengths of light. The difference in wavelengths for each element allows to identify element species in the material and also quantitatively measure the amounts of elements in the sample. The spot size of LIBS is about 30~200 μm, which is appropriate to observe electrode level. In addition, depth profiling of the sample can be conducted because once the laser is induced, the sample is shaved to a thickness of several tens of micrometers.

2.3 Scanning electron microscopy

Morphology change of active materials was observed by Scanning electron microscopy (SEM, SU70, Hitachi, and SUPRA). In case of observing the active particles near the separator, the top side of electrode was speculated. On the other hand, for the particles near the current collector, the electrode materials located upper side was eliminated by Kapton tape, and the top side of the remained electrode was observed.

2.4 X-ray photoelectron spectroscopy

The amounts of electrolyte decomposition were measured by X-ray photoelectron spectroscopy. The binding energy was referenced to the C 1s peak at 284.5 eV. To observe the active particles near the separator, the top side of electrode was conducted. In case of the active particles near the current collector, the electrode materials being upper side was uncovered by Kapton tape, and the top side of the remained electrode was observed.

2.5 Electrochemical impedance spectroscopy

Electrochemical impedance spectroscopy (EIS) analysis was conducted after the Li/NCM622 cell was charged to 4.3 V every 20 cycles. A sine-modulated AC potential of 10 mV was applied in the frequency range of 200 kHz to 5 mHz.

2.6 X-ray diffraction

The electrodes were analyzed using a X-ray diffractometry (XRD, D2 PHASER, Bruker, Bremen, Germany) equipped with Cu-Kα (λ = 1.54178). In case of observing the active particles near the separator, the top side of electrode was analyzed. On the other hand, for the particles near the current collector, the electrode materials located upper side were carefully eliminated by taping method until the Aluminum current collector peaks were obtained (Figure 7).

Chapter 3. Results and discussion

3.1. Effect of electrode thickness on cyclability

Two different loading levels of $LiNi_{0.6}Co_{0.2}Mn_{0.2}O_2$ (NCM622) were prepared, and their cross-section images of Scanning electron microscopy (SEM) are shown in Figure 1. The thickness of normal loading level electrode (20 mg cm^{-2}, N20) is about 70 μm, and high loading level electrode (28 mg cm^{-2}, H28) is nearly 100 μm. After preparation of electrodes, their cyclability tests were carried out and the results are shown in Figure 2. The initial areal capacity of H28 was 4.2 mAh cm^{-2}, which was 1.4 times higher than 3.0 mAh cm^{-2} of N20, and the initial specific capacities of both electrodes were almost same, 150.1 mAh g^{-1} of N20, and 149.9 mAh g^{-1} of H28. After 100 cycles, however, the capacity retention of H28 was 36 %, which was much lower than 76 % of N20. These results reveal that thick and normal electrodes operate the same during the early stages of cycles, but the capacity retention of H28 severely deteriorates during the later stages of cycles. Among the various factors that can affect the cyclability, the major difference between the two electrodes is the elongated charge carrier pathways. In this regard, one of the two paths could be the rate-determining-step of H28, Li^+ ion transport through the electrolyte which is penetrated in the electrode or electron transport via conducting agents (Figure 3). In case of the ion transport, the active materials near the current collector is hard to be fully utilized because it is the farthest side from the anode. On

the contrary, for the electron transport, the active particles near the separator become inactive because its pathway is the longest from the current collector. Consequently, the thick electrode can cause the state of charge (SOC) inhomogeneity in the electrode level due to the elongated pathways which contribute to sluggish charge carrier transport kinetics.

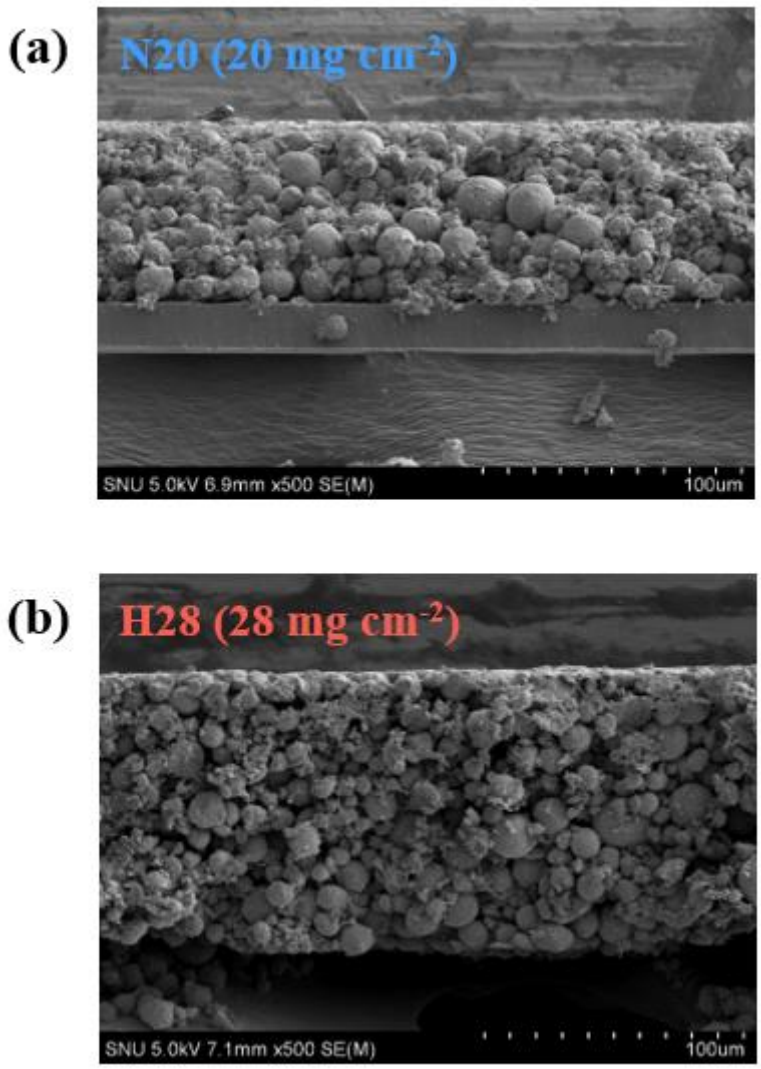

Figure 1. Cross-section SEM image of (a) N20 and (b) H28.

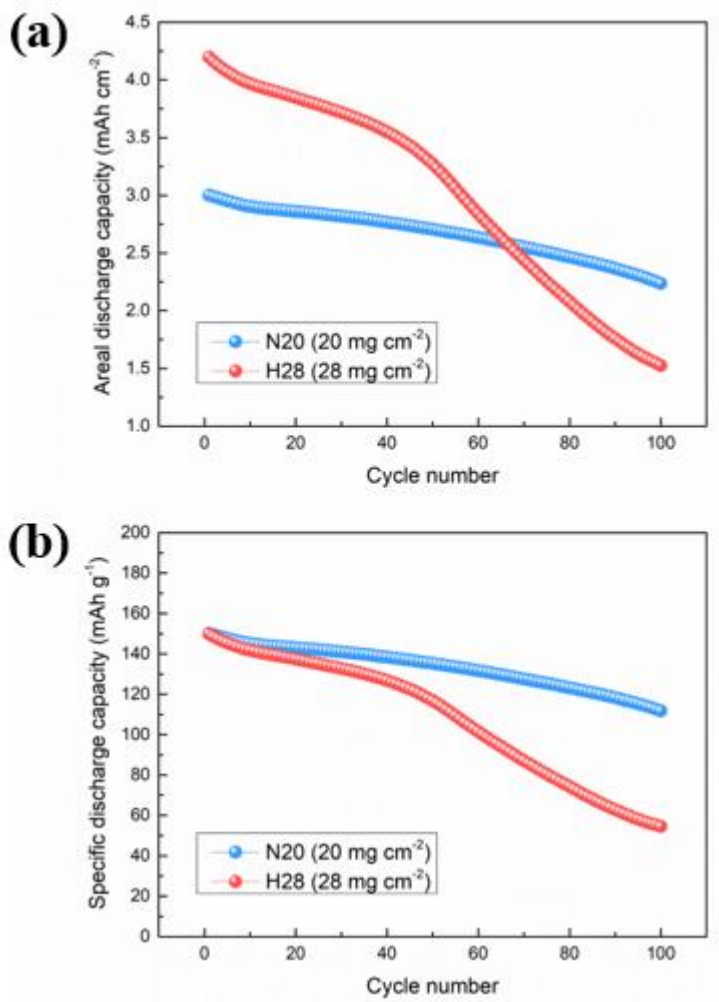

Figure 2. Comparison with cycle life of N20 (blue) and H28 (red) in terms of (a) areal discharge capacity and (b) specific discharge capacity.

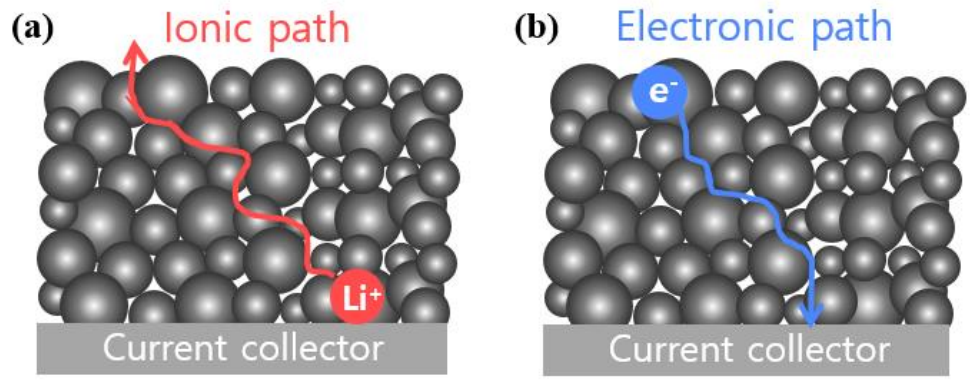

Figure 3. Two types of charge carrier pathways on charge. (a) Li-ion transport through electrolyte impregnated in the electrode (b) electron transport via conducting agent. On discharge, the directions are reversed.

3.2. State of charge inhomogeneity in electrode level

The SOC differences in the electrode along the thickness were qualitatively confirmed by Laser induced breakdown spectroscopy (LIBS). LIBS is an effective apparatus for quantifying Lithium amount because LIBS is highly sensitive to detect Lithium as shown in Figure 4(a). In addition, it is appropriate to observe electrode level due to its large and controllable spot size (30~200 μm), and also depth profiling of the sample can be conducted with thickness of several tens of micrometers. The depth profiling was operated until notable Aluminum peak is observed in the intensity profile of LIBS (Figure 4(b)). To figure out SOC inhomogeneity in electrode level, the spot size and laser intensity were properly adjusted to reach the current collector in about tenth shot for each case of N20 and H28. Furthermore, the SOC was decided to relative lithium quantity, which is a ratio of lithium intensity per sum of transition metal intensities, and the quantities of each shot was normalized by the quantity of the first step that represents a side of near the separator.

$$Relative\ \ lithium\ \ quantity = \frac{Li\ \ intensity}{Ni + Co + Mn\ \ intensity}$$

Figure 5 is a result of depth profiling for pristine electrode, and there was no significant deviance of lithium amount from separator side to current collector side. On the other hand, as the cycles progressed, there was a different trend of SOC distribution between N20 and H28. To confirm the trend of SOC changes as a function of thickness during the cycling, the 4.3 V-charged electrodes were collected for every 25 cycles (Figure 6). In case of charged state for N20, the distribution was

rarely changed as cycle number increased. However, in case of charged state for H28, the amounts of lithium were increased, especially near the current collector. This result indicates that the active particles located near current collector become inactive during the cycling, while active particles near separator actively oxidize/reduce during the cycling. To confirm the SOC inhomogeneity quantitatively, the changes of lattice parameters after cycling were analyzed by using X-ray diffraction (XRD) and full pattern matching method. Before measuring the XRD, I simply tested the penetration depth of X-rays by using a thinner electrode. In the case of 50 μm thickness electrode with a loading level of 14 mg cm^{-2}, Aluminum (current collector) peaks (Figure 7(b)) were not detected as shown in Figure 7(a). This result reveals that the penetration depth of X-ray is shorter than 50 μm for the whole measurement two-theta range. Thus, I concluded that the information of XRD on electrode surface can represent the separator part less than 50 μm thickness of electrode (Figure 7(c)). In case of the XRD measurement of the current collector part, the active materials being upper side are carefully peeled off by taping method until I obtained the peaks of Al current collector (Figure 7(d)), which means that the XRD patterns for bottom part of electrode is obtained with less than 50 μm thickness. Figure 8 shows the results of XRD after every 25 cycles with surface part and bottom part of electrodes. In case of N20s, there were little differences between the peaks of the separator and current collector part after the cycling. It means that the degradation of electrochemical performances is mainly attributed to the active materials itself rather than electrode thickness. On the other hand, in case of H28,

the positions of peaks were clearly mismatched between the separator and current collector part, especially in 50th, 75th, and 100th cycled electrode. The (108) and (110) peaks of the separator parts became more split, and the (113) peak of the separator part became more shifted to right side than the current collector parts after the cycling on the charged state. On the discharged state, the trends were reversed that the separator part of active materials has more discharged state than the current collector part. These results clearly show that the active materials being the separator part were more actively participating in the electrochemical reaction than the active materials being the current collector part as increased the cycle numbers[20]. The lithium quantities of each separator and current collector part every 25 cycles were calculated from the lattice parameters by full pattern matching method (Figure 9). In case of N20, it was slightly decreased that the difference of lithium quantities between charge/discharge of both the separator and current collector part as the cycle number increased. On the other hand, in case of H28, the difference was more severely decreased on the current collector part than the separator part. This result is well agreement in the LIBS data (Figure 6) that the active materials near the current collector become more exploited in the electrochemical reaction as the cycle increased in case of H28. These results well support that the rate-determining-step of thick electrode is Li^+ transport through electrolyte impregnated in the electrode rather than electron transport via conducting agents. The trend of SOC distribution is clearly different between N20 and H28, the severe SOC inhomogeneity of H28 is a possible major factor of capacity fading.

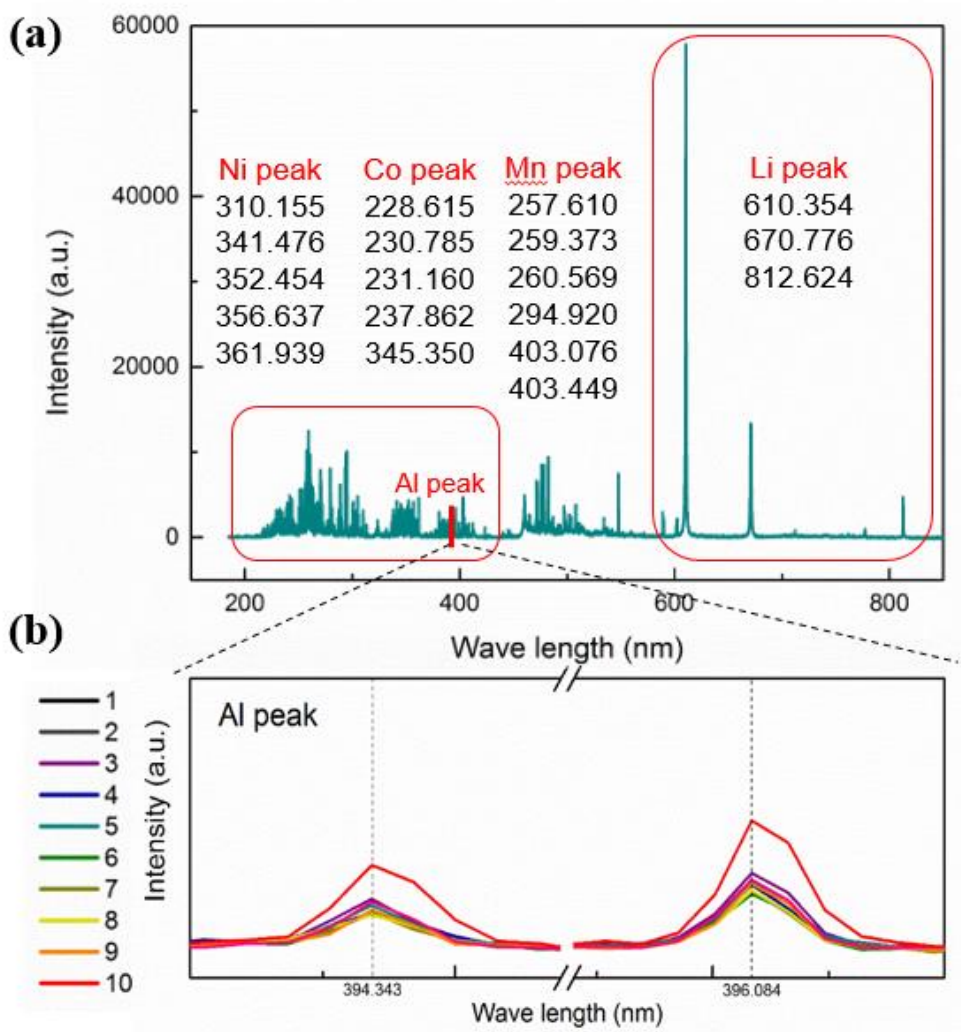

Figure 4. (a) LIBS intensity profile of pristine NCM622 electrode. (b) Magnified peaks of Aluminum from first to tenth shot.

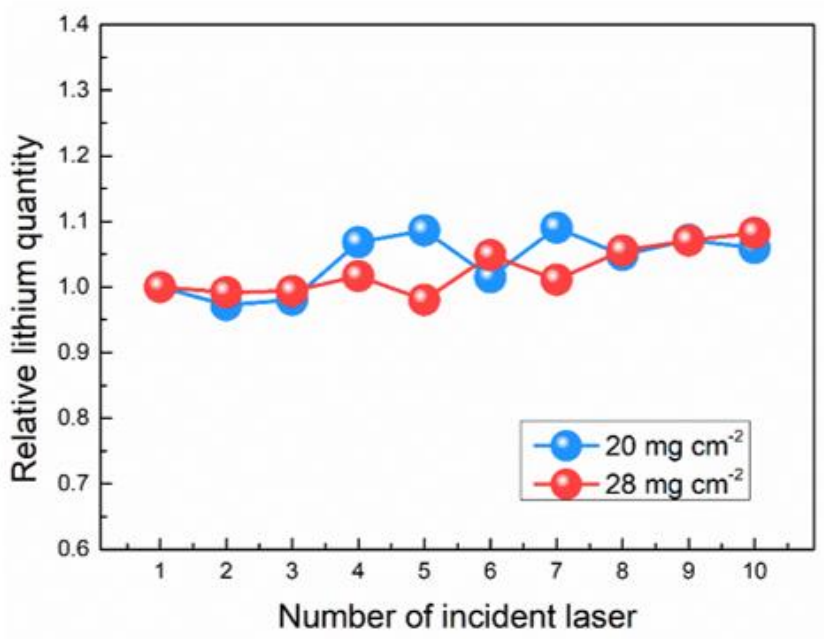

Figure 5. LIBS depth profiling results of pristine N20 (blue) and H28 (red).

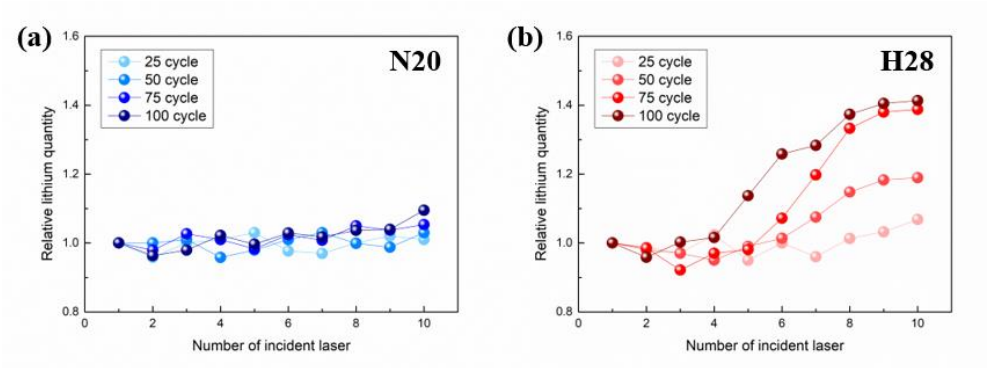

Figure 6. State of charge inhomogeneity in electrode level after charged every 25 cycles. (a) N20. (b) H28.

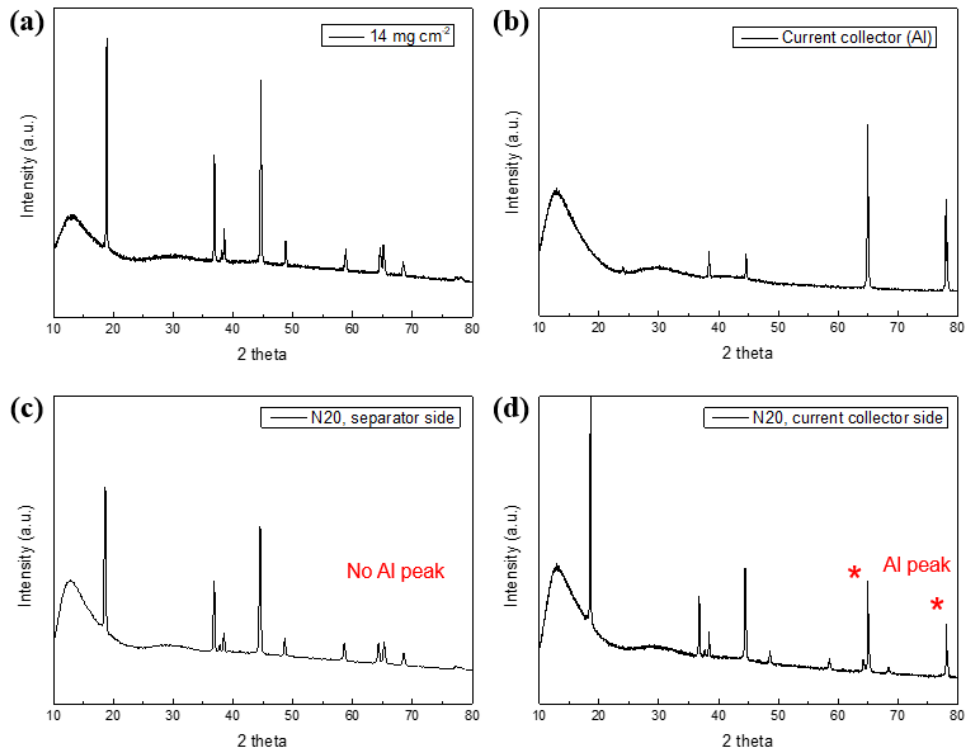

Figure 7. XRD patterns of (a) pristine 14 mg cm^{-2} electrode, (b) Aluminum current collector, (c) separator side of N20, and (d) current collector side of N20.

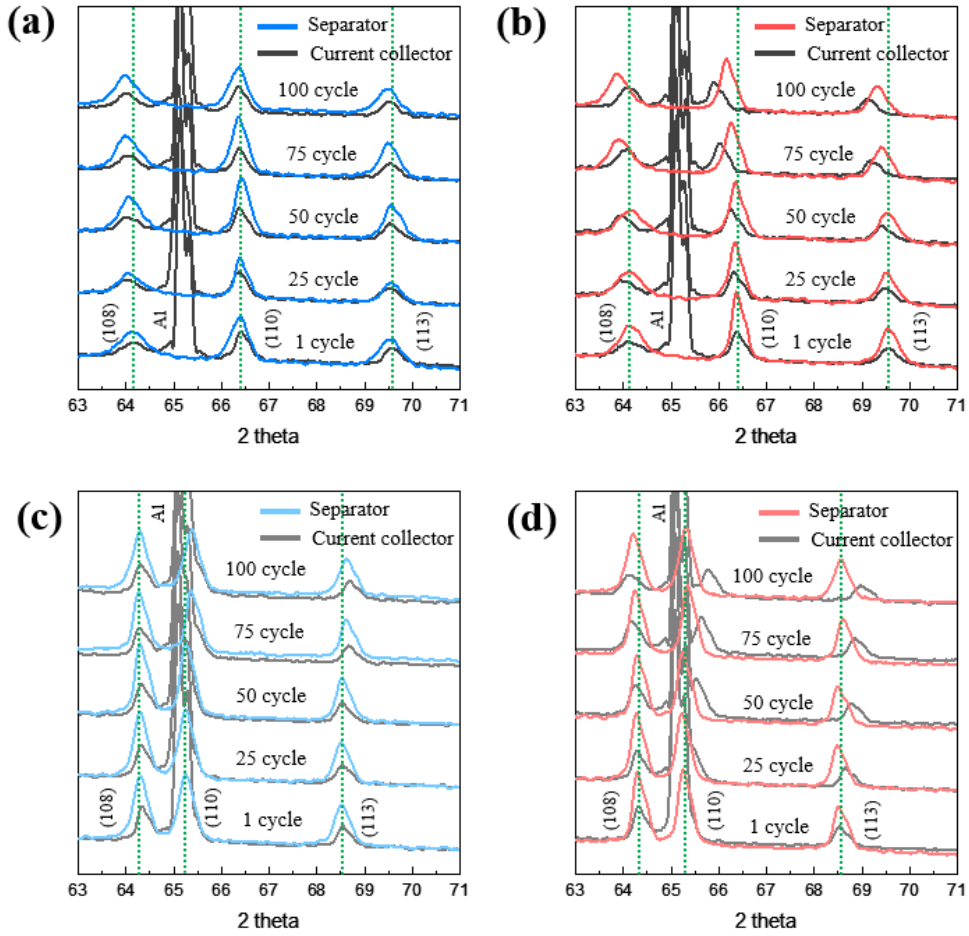

Figure 8. Ex-situ XRD patterns every 25 cycles. The patterns of separator and current collector side were overlaid. (a) After charged, N20. (b) After charged, H28. (c) After discharged, N20. (d) After discharged, H28. There were no Al peaks on the patterns of the separator sides, while they were clearly observed on the patterns of the separator side

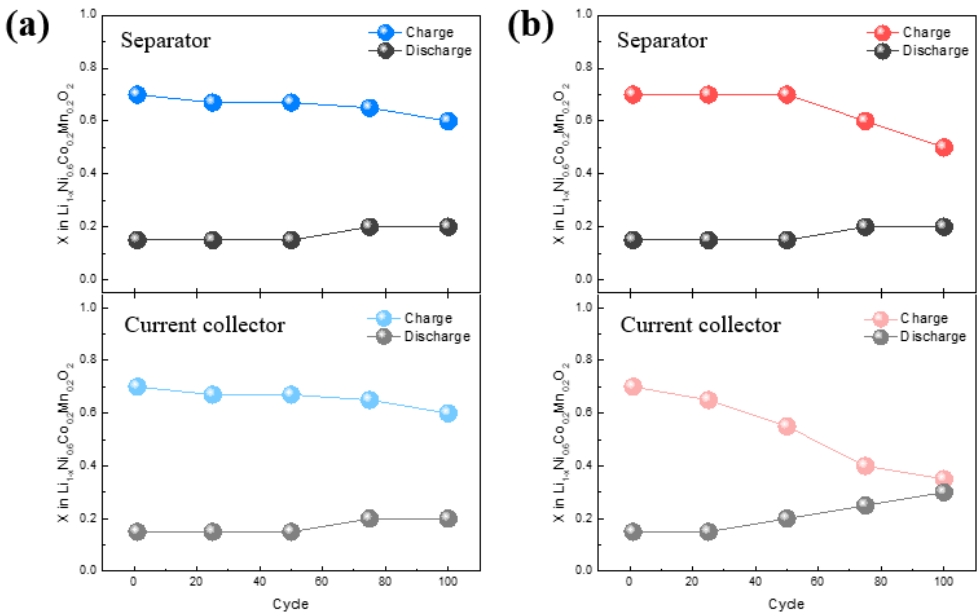

Figure 9. The calculated Li quantities from lattice parameter by full pattern matching method every 25 cycles. (a) N20. (b) H28.

3.3. Uneven degradation behavior at electrode scale

To verify the relationship between the uneven SOC and cell degradation, the morphology of the active particles near the separator and current collector were captured by Scanning Electron Microscopy (SEM, Figure 10). After 100 cycles, there were no significant cracks on the secondary active particles near the separator and current collector of N20. However, in case of H28, the secondary particles near the separator were cracked severely, while the particles near the current collector were intact. Those cracks could contribute to decreasing battery performance in many ways such as electrolyte decomposition by producing additional cathode-electrolyte-interphase (CEI layer), and increasing charge-transfer resistance from new surface areas generated by crack[17]. X-ray photoelectron spectroscopy (XPS, Figure 11) was conducted for quantifying the amount of electrolyte by-products. The C 1s spectra in Figure 11 shows that the ratio of the three peaks at 289, 286, and 284.5 eV, corresponding to C=O, C-O, and conducting agent in the 100 cycled electrode, respectively. In case of N20, the difference between the separator and current collector side was negligible. On the other hand, for H28, notable discrepancy between the separator and current collector side was obtained. The C=O and C-O peaks of the separator side was larger than the current collector side with respect to the peaks of conducting agent. This result indicates that the electrolyte decomposition is generated more vigorously near the separator side than the current collector side in case of H28, because the peaks of C=O and C-O represent the amount of electrolyte by-products[19]. Furthermore, the impedances were measured by

Electrochemical impedance spectroscopy analysis (EIS, Figure 12). In case of N20, the impedance was increased slightly after every 20 cycles, whereas in case of H28, the rate of increment was remarkable. After the 80 cycles progressed, merely 76 % impedance of N20 was increased, while the impedance of H28 was developed to 180%. Accordingly, in case of thick electrode which showed inhomogeneous SOC during the cycling, there were detrimental side effects, such as crack and electrolyte by-products in electrode level. On the other hand, the normal thickness electrode, which maintained homogenous SOC during the cycles, did not exhibit significant cracks or electrolyte by-products in electrode level.

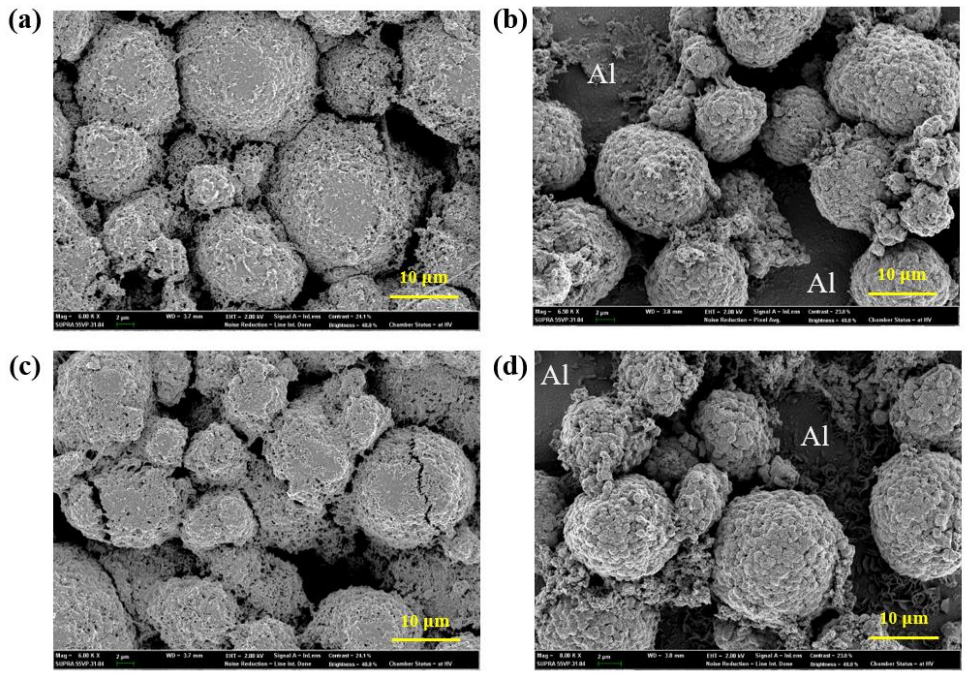

Figure 10. SEM images of secondary active particles after 100 cycles. (a) N20, separator side. (b) N20, current collector side. (c) H28, separator side. (d) H28, current collector side.

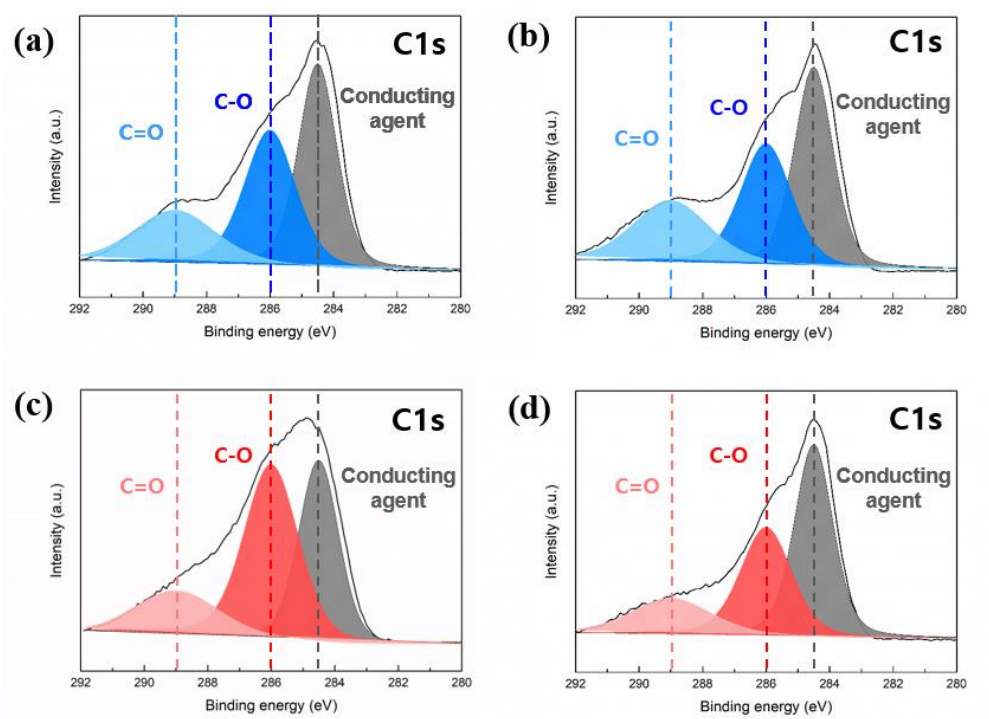

Figure 11. The amount of electrolyte by-products measured by XPS after 100 cycles. (a) N20, separator side. (b) N20, current collector side. (c) H28, separator side. (d) H28, current collector side.

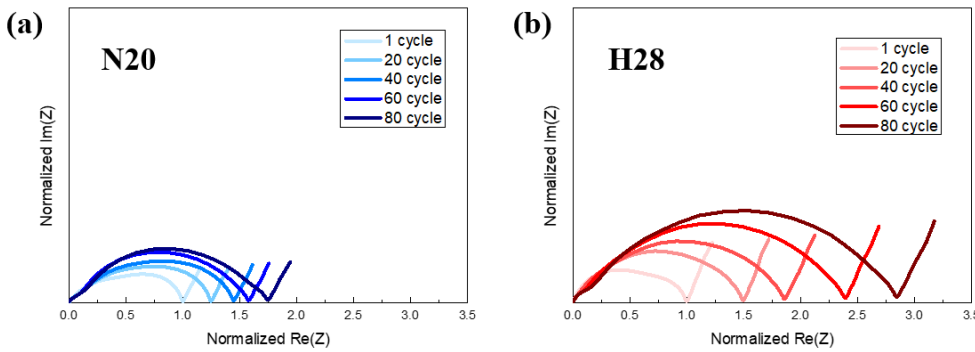

Figure 12. Impedance measurements every 20 cycles by EIS for (a) N20 (b) H28.

3.4. Capacity fading mechanism of thick electrode

The capacity of H28 is severely faded after cycling compared with N20 electrode, and I observed that the active particles near the separator part are degraded significantly which operates more vigorously than the active particles near the current collector. This situation can be possibly originated from the effective current density. The effective current density of the separator sides (*i.e.* the rate of SOC change) is higher than the current collector side, because the ΔSOC of the separator side is higher than the current collector side and the electrode is operating at constant-current mode (CC). To figure out the correlation between current density and capacity retention, I prepared an electrode whose loading level is 14 mg cm^{-2}. Its cyclability test was conducted at three different current densities; 150 mA g^{-1}, 300 mA g^{-1}, and 750 mA g^{-1} (Figure 13). It was observed that the capacity retention became faded severely with the current density increase. Therefore, the degradation on the active particles near separator of H28 is accelerated by the increment of the current density. The uneven effective current density is induced by the combination of degraded electrode structure and the sluggish ion transport in electrolyte, *i.e.,* not enough time to utilize active particles near the current collector part. To support this claim, a cycle test with constant-current and constant-voltage mode (CCCV) was conducted to supply enough time to Li^+ diffusion (Figure 14, Experimental section). Interestingly, the capacity retentions of N20 were similar for both CCCV and CC modes, which supports that the degradation of N20 electrode is not attributed to the electrode inhomogeneous after cycling. However, the capacity retention of H28 for

CCCV mode was much higher than CC mode, and even comparable with the capacity retention of N20. This result support that the SOC and current density inhomogeneity is originated from sluggish ion transport and elongated Li^+ diffusion paths after cycling as the major factors of the capacity fading. Consequently, the Li^+ ion transport pathway through the electrolyte penetrated in the electrode of H28 is elongated due to its high loading level. This elongated path causes uneven SOC that the active particles near the current collector become unutilized, while active particles near the separator are vigorously utilized. For this reason, the active particles near the separator manage higher SOC and current density than near the current collector ones. These situations allow the active particles near the separator to be cracked and suffer from the electrolyte by-products. Moreover, Y. Oumellal *et al.* reported that tortuosity of porous electrode can be elevated by products of electrolyte decomposition, and the increased tortuosity hinders Li^+ ion diffusion[19]. As a result, the active particles near the current collector become more inactive than the earlier stage of cycles, and the capacity fading of thick electrode is boosted (Figure 15).

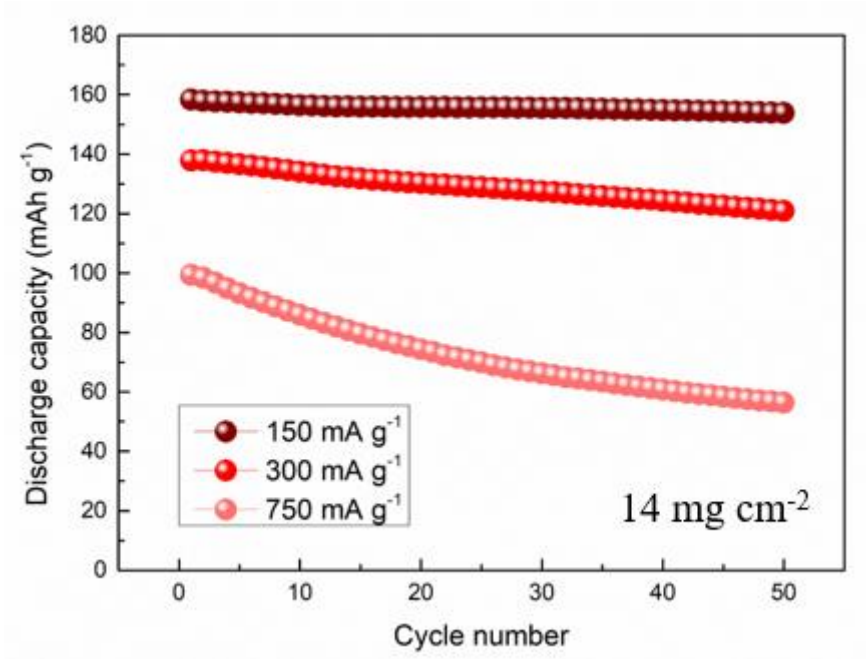

Figure 13. Cyclability test with different current density.

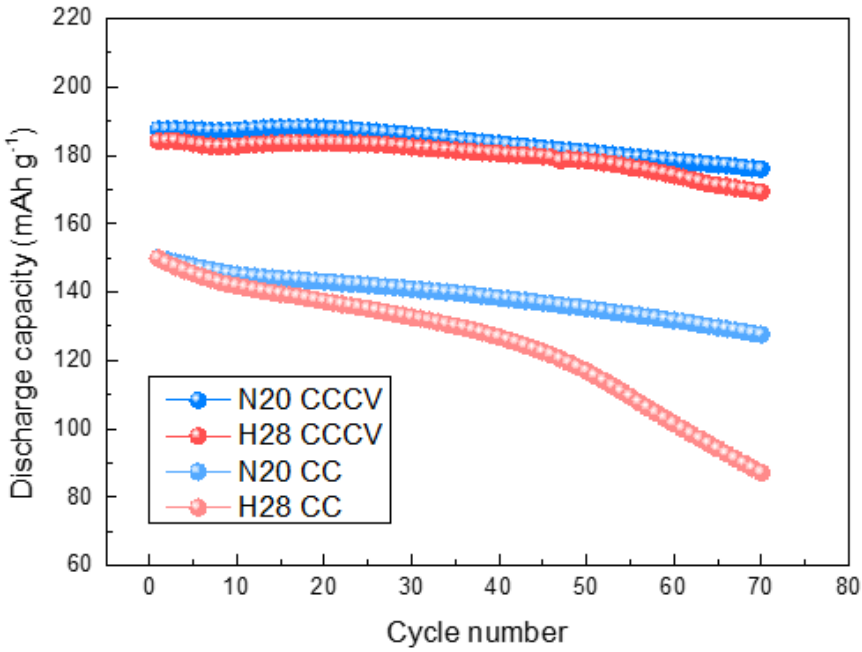

Figure 14. Cyclability test with different charge/discharge protocols. The upper part is for constant-current and constant-voltage mode (CCCV). The lower part is for constant-current mode (CC).

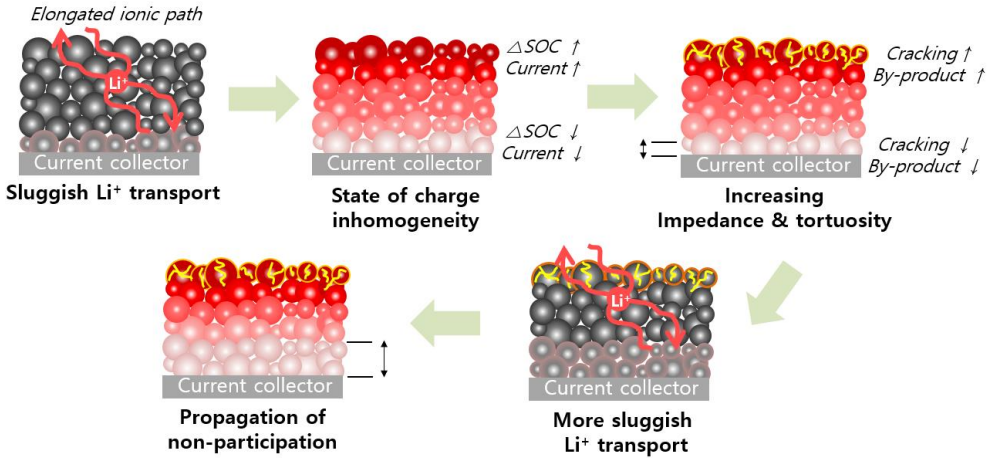

Figure 15. Suggested the capacity fading mechanism of thick electrode.

Chapter 4. Conclusion

In summary, two types of electrodes with different loading level were prepared to compare cycle life of thicker electrode. After 100 cycles, the capacity of the thick electrode (H28, 28 mg cm^{-2}) was deteriorated significantly than the normal electrode (N20, 20 mg cm^{-2}). To verify the factors affecting different cycle life, the trends of SOC inhomogeneity in the electrode level during the cycle was obtained by LIBS and XRD. As the cycles progressed, in case of N20, there were negligible differences of SOC distribution, while the amount of unutilized active particles near the current collector of H28 was increased. The degradation behaviors of the active particles were also confirmed by SEM, XPS, and EIS. There was no considerable uneven degradation in the electrode level of N20 during the cycling. On the other hand, it was observed that the active particles near the separator were severely deformed than near the current collector ones in case of H28. Consequently, these situations produced the increased impedance and tortuosity of H28, and capacity fading of thick electrode was accelerated. I believe that these findings are expected to be a critical role in solving the issues of thick electrode and contribute to developing high energy density battery.

References

[1] A. Yoshiho, *Angew. Chem. Int. Ed.,* **2012,** 15, 5798

[2] M. Armand, J.-M. Tarascon, *Nature,* **2008,** 451, 652

[3] H.-D. Lim, B. Lee, Y. Bae, H. Park, Y. Ko, H. Kim, J, Kim, K. Kang, *Chem. Soc. Rev.,* **2017,** 46, 2873

[4] Y. Bae, H. Park, Y. Ko, H, Kim, S. K. Park, K. Kang, *Batteries & Supercaps*, **2019,** 2, 1

[5] W. Kang, N. Deng, J. Ju, Q. Li, D. Wu, X. Ma, L. Li, M. Naebe, B. Cheng, *Nanoscale,* **2016,** 8, 16541

[6] S. Lee, G. Kwon, K. Ku, K. Yoon, S.-K. Jung, H.-D. Lim, K. Kang, *Adv. Mater.,* **2017,** 30, 1704682

[7] J. Billaud, F. Bouville, T. Magrini, C. Villevieille, A. Studart, *Nature Energy,* **2016,** 1, 16097

[8] J. S. Sander, R. M. Erb, L. Li, A. Gurijala, Y.-M. Chiang, *Nature Energy,* **2016,** 1, 16099

[9] C.-J. Bae, C. K. Erdonmez, J. W. Halloran, Y.-M. Chiang, *Adv. Mater.,* **2013,** 25, 1254

[10] K. Evanoff, J. Khan, A. A. Balandin, A. Magasinski, W. J.

Ready, T. F. Fuller, G. Yushin, *Adv. Mater.,* **2012,** 24, 533

[11] M. Singh, J. Kaiser, H. Hahn, *J. Electrochem. Soc.,* **2015,** 162, 7

[12] R. Zhao, J. Liu, J. Gu, *Appl. Energy,* **2015,** 139, 220

[13] J. Newman, *J. Electrochem. Soc.,* **1995,** 142, 97

[14] M. Singh, J. Kaiser, H. Han, *Batteries,* **2016,** 2, 35

[15] K. Kitada, H. Murayama, K. Fukuda, H. Arai, Y. Uchimoto, Z. Ogumi, E. Matsubara, *J. Power Sources,* **2016,** 301, 11

[16] Z. Du, D. L. Wood, C. Daniel, S. Kalnaus, J. Li, *J. Appl. Electrochem.,* **2017,** 47, 405

[17] S. Watanabe, M. Kinoshita, T. Hosokawa, K. Morigaki, K. Nakura, *J. Power Sources,* **2014,** 258, 210

[18] Y. Oumellal, N. Delpuech, D. Mazouzi, N. Dupre, J. Gaubicher, P. Moreau, P. Soundan, B. Lestriez, D. Guyomard, *J. Mater. Chem.,* **2011,** 21, 6201

[19] L. Yang, B. Ravdel, B. L. Lucht, *Electrochem. Solid-State Lett.,* **2010,** 13, 95

[20] W. Lee, S. Muhammad, T. Kim, H. Kim, E. Lee, M. Jeong, S.

Son, J.-H. Ryou, W.-S. Yoon, *Adv. Energy. Mater.,* **2018,** 8, 1701788

국문요약

실용적인 관점에서 전극의 후막화는 배터리의 에너지 밀도를 높이는데 효과적인 방법이 될 수 있다. 이는 단위 면적 당 전극 활물질을 두껍게 적층함으로써 상대적으로 집전체, 분리막, 케이스와 같은 비활성 물질의 비율을 최소화 하는 방식으로 에너지 밀도 향상에 기여한다. 하지만 이와 같이 전극의 두께가 증가하게 되면 배터리의 수명이 급격하게 감소하게 된다. 기존 두께의 전극과 후막 전극의 차이는 오직 전하 전달 물질의 확산경로가 증가하는 것이기 때문에 후막 전극의 경우 활물질의 위치에 따라 전하 전달 물질이 효과적으로 확산되기 힘든 상황이 발생할 수 있다. 만일 리튬 이온의 확산이 저해되는 것이라면 음극으로부터 거리가 먼 집전체 부근의 활물질이 비활성화 될 것이며, 전자의 전달이 어려워지는 것이라면 집전체로부터 거리가 먼 곳에 위치한 분리막 부근의 활물질이 비활성화 될 것이다. 이에 따라 본인은 전극의 두께와 배터리의 수명이 열화되는 기작에 대하여 알아보기 위해 먼저 LIBS라는 장비를 통하여 사이클이 진행됨에 따라 전극단위 충전상태의 불균일성을 측정하였다. 그 결과, 기존 전극은 사이클이 진행되어도 전극단위 충전상태가 균일한 반면, 후막 전극의 경우 집전체 부근의 활물질이 점점 비활성화되는 것을 관측하였다. 이는 곧 전극 내 함침 되어있는 전해질을 통한 리튬이온의 확산이 증가된 경로로 인해 원활히 일어나지 못함을 의미

한다. 또한 이러한 전극의 전극단위 충전상태 불균일성과 수명이 열화되는 것의 상관관계를 알아내기 위하여 SEM, XPS, EIS와 같은 장비를 통하여 분리막 부근과 집전체 부근 활물질의 열화정도를 분석하였다. 그 결과, 100사이클이 지난 이후, 기존 전극의 경우에는 100사이클이 지나도 분리막 부근과 집전체 부근의 활물질 모두 크게 열화가 되지 않았다. 이에 반해 후막 전극의 경우에는, 분리막 부근의 활물질은 파쇄가 되고 전해질의 부산물들이 쌓여 있는 반면, 집전체 부근의 활물질은 초기 상태와 크게 다르지 않음을 발견하였고 이러한 결과는 곧 후막 전극의 전체적인 저항의 증가로 이어졌다. 분리막 부근의 활물질이 파쇄되며 전해질 부산물이 쌓이게 되면, 전해질을 통한 리튬 이온의 확산이 더욱 어려워지게 되고, 이에 따라 집전체 부근의 활물질은 더욱 비활성화가 되기 때문에 후막 전극의 수명이 급격하게 저하되는 것이다. 본 연구의 결과는 후막 전극 성능을 개선시킬 수 있는 방안을 고안함에 있어서 핵심적인 초석이 될 것으로 기대되며 그로 인하여 고 에너지 밀도의 배터리를 개발하는 데 있어 중요한 역할을 할 것으로 예상된다.

주요어: 리튬 이온 이차 전지, 층상 구조 산화물, 후막 전극, 전극단위 충전상태 불균일성, 수명 열화

학 번: 2017-29935